DOI: 10.13009/EUCASS2023-357
Aerospace Europe Conference 2023 – 10TH EUCASS – 9TH CEAS

Explicit Midcourse Guidance Law of Multi-stage Anti-ballistic Missile with Solid Propellant

Yeontaek Jung[⋆†], *Hanna Lee*[⋆], *Youngjun Lee*[⋆], *and Youdan Kim*[⋆]
[⋆]*Department of Aerospace Engineering, Seoul National University*
Seoul 08826, Republic of Korea
{skfmsgka, hn.lee, josj80, ydkim}@snu.ac.kr
[†]Corresponding author

Abstract

This study presents a midcourse guidance law designed for the second last stage of the multi-stage anti-ballistic missile. The structure of the guidance command is obtained through an optimal control problem, allowing for the prediction of the time-to-go. Subsequently, the guidance command is computed using the predicted time-to-go. The proposed guidance law adopts a feedback strategy that does not require pre-computed data. To assess the effectiveness of the proposed guidance law, numerical simulations are conducted, and a comparative analysis with the modified zero-effort-miss guidance law is provided. The proposed guidance law is evaluated considering two key performance metrics: the miss distance and the interceptor's speed at the interception point.

1. Introduction

The threat of ballistic missiles has increases the significance of anti-ballistic missile systems in the defense system. The interception altitude of anti-ballistic missiles depends on the types of the ballistic missiles, but normally it is assumed that interception occurs in the exo-atmospheric region.[1] To achieve interception at high altitudes, anti-ballistic missiles typically consists of three or four stages. In the case of multi-stage anti-ballistic missiles, the guidance law implemented in the preceding stages significantly impacts the guidance law's performance of the subsequent stages. Unsuccessful positioning with adequate velocity of the anti-ballistic missile at the former stages results in excessive guidance commands during the terminal phase, which may lead to interception failure. Consequently, the development of a suitable guidance law for the middle stage of the multi-stage anti-ballistic missiles is very important.

Various research have been conducted on midcourse guidance laws for the last stage with solid propellant. Newman proposed the Modified Zero-Effort-Miss (MZEM) guidance law, which incorporates the line of sight direction vector and Zero-Effort-Miss (ZEM).[2] ZEM represents the relative position of the target, i.e., ballistic missile, with respect to the interceptor, i.e., anti-ballistic missile, when their distance is at a minimum. Zes employed the Kepler problem and the J2 gravity model to calculate ZEM,[3] while Ann et al. solved the optimal trajectory problem to address the limitation of ZEM-based guidance laws.[4] Du et al. and Zhao et al. utilized a velocity-to-be-gained derived from the Lambert problem.[5,6]

Conversely, midcourse guidance laws for stages preceding the last stage generally employ optimal control problems. Due to the computational demands associated with solving these problems in real-time, they are typically computed at ground stations prior to launch. To enhance response time, tables of optimal trajectories[1,7] or learning-based algorithms[8–10] are employed. However, these methods necessitate extensive data to handle various engagement scenarios.

In this study, a midcourse guidance law is designed especially for stages preceding the last stage, which obviates the need for pre-computed data and employs a feedback strategy. To predict the intercept point, the guidance command structure is derived from an optimal control theory. By utilizing this structure, time-to-go is predicted, and the guidance command is computed. The performance of the proposed guidance law is compared with that of the MZEM guidance law, which also does not require pre-computed data. Numerical simulations are conducted to evaluate the performance of both guidance laws with respect to miss distance and interceptor speed at the intercept point. It is important to note that interceptor speed plays a crucial role in enhancing kill probability, because the interceptor relies on kinetic energy to kill the target. The interceptor considered in this study has three stages with solid propellant and an exo-atmospheric kill vehicle. Thus, the proposed guidance law is applied to the second stage with solid propellant in the numerical simulations.

DOI: 10.13009/EUCASS2023-357

The remainder of this paper is organized as follows: Secion 2 provides the equations of motion utilized in the numerical simulations. In Sec. 3, guidance law of the second last stage of the anti-ballistic missile is proposed. Numerical simulation results are presented in Sec. 4. Finally, Sec. 5 concludes the paper.

2. Equations of Motion

The interceptor considered in this study is modeled as a point mass system with three degrees of freedom. The dynamic equations of a interceptor can be represented as follows,[11]

$$\frac{dm}{dt} = -\frac{T_{vac}}{g_0 I_{sp}} \tag{1}$$

$$\frac{dr}{dt} = V \sin\gamma \tag{2}$$

$$\frac{d\Lambda}{dt} = \frac{V\cos\gamma\sin\chi}{r\cos\lambda} \tag{3}$$

$$\frac{d\lambda}{dt} = \frac{V\cos\gamma\cos\chi}{r\cos\lambda} \tag{4}$$

$$\frac{dV}{dt} = \frac{T\cos\alpha\cos\beta - D}{m} - \frac{\mu_e\sin\gamma}{r^2} + r\omega_e^2\cos\lambda(\sin\gamma\cos\lambda - \cos\gamma\sin\lambda\cos\chi) \tag{5}$$

$$\frac{d\gamma}{dt} = \frac{T\sin\alpha + L}{mV} + \frac{(rV^2 - \mu_e)\cos\gamma}{r^2 V} + \frac{r\omega_e^2\cos\lambda}{V}(\cos\gamma\cos\lambda + \sin\gamma\sin\lambda\cos\chi) + 2\omega_e\cos\lambda\sin\chi \tag{6}$$

$$\frac{d\chi}{dt} = -\frac{T\cos\alpha\sin\beta + Y}{mV\cos\gamma} + \frac{V}{r}\cos\gamma\tan\lambda\sin\chi + \frac{r\omega_e^2}{V\cos\gamma}\sin\lambda\cos\lambda\sin\chi + 2\omega_e(\sin\lambda - \tan\gamma\cos\lambda\cos\chi) \tag{7}$$

where m is the mass of the interceptor, r is the distance from the center of the Earth, Λ is a longitude, λ is a latitude, V is the relative speed of the interceptor with respect to the rotating Earth, γ is a flight path angle, and χ is a flight azimuth angle. T_{vac} is a thrust at vacuum, g_0 is a gravitational acceleration at the sea level, I_{sp} is a specific impulse at vacuum, ω_e is the angular velocity of the Earth, and μ_e is the standard gravitational parameter of the Earth. L, D, Y are lift, drag, sideforce of aerodynamic forces, and T is a thrust, which are modeled as follows,

$$L = F_N\cos\alpha - F_A\cos\alpha \tag{8}$$

$$D = F_N\sin\alpha + F_A\cos\alpha \tag{9}$$

$$L = \frac{1}{2}\rho V^2 S C_{N,\beta} \tag{10}$$

$$T = T_{vac} - A_e p(h) \tag{11}$$

with

$$F_A = \frac{1}{2}\rho(h)V^2 S C_A \tag{12}$$

$$F_N = \frac{1}{2}\rho(h)V^2 S C_{N,\alpha} \tag{13}$$

$$p(h) = p_0 e^{-h/h_0} \tag{14}$$

$$\rho(h) = \rho_0 e^{-h/h_0} \tag{15}$$

where A_e is the area of nozzle exhaust exit, S is a reference surface area, C_A is an axial force coefficient, C_N is a normal force coefficient, $p(h)$ is the pressure of the air, ρ is the density of the air, and h is the altitude of the interceptor.

Because the interceptor is modeled as a point mass system, it is assumed that the attitude of the interceptor is controlled to align the desired thrust direction. Therefore, the angle of attack, α, and the sideslip angle, β, are control variables. Also, the total angle of attack is defined as follows,

$$\alpha_{total} = \cos^{-1}\frac{\boldsymbol{v}_I^T\hat{\boldsymbol{u}}}{||\boldsymbol{v}_I||_2} \tag{16}$$

where $\hat{\boldsymbol{u}}$ is a unit vector representing thrust direction. The guidance command, represented as thrust direction command, will be converted to the angle of attack and sideslip angle in the numerical simulation. Note that the total angle of attack represents how excessively the interceptor maneuvers to follow the guidance command.

DOI: 10.13009/EUCASS2023-357

The target is assumed that it is in free flight, which means that the gravitational force only affects the motion of the target. The equations of motion governing the target can be written as follows,

$$\dot{\boldsymbol{r}}_T = \boldsymbol{v}_T \tag{17}$$

$$\dot{\boldsymbol{v}}_T = \boldsymbol{g}(\boldsymbol{r}_T) \tag{18}$$

with

$$\boldsymbol{g}(\boldsymbol{r}) = -\frac{\mu_e}{||\boldsymbol{r}||_2^3}\boldsymbol{r} \tag{19}$$

where $\boldsymbol{g}(\cdot)$ is the gravitational acceleration, and $||\cdot||_2$ is the Euclidean norm of a vector.

3. Guidance Law

This section explains the proposed guidance law, which consists of prediction of the interceptor and computation of the guidance command. The Predicted Interceptor Point (PIP) represents the location on the target's trajectory where both the target and interceptor are expected to arrive simultaneously. The target is assumed to be in free flight during engagement. Therefore, it is very important to accurately predict the time-to-go so that the interceptor may reach the predicted interceptor point. Note that the accuracy of time-to-go prediction is influenced by the guidance law. Therefore, in this study, the structure of guidance law is designed, and then the time-to-go is predicted. Then, guidance command is computed.

3.1 Structure of Guidance Law

The structure of the guidance law is derived from the following optimal control problem.

$$\min_{\hat{\boldsymbol{u}}} J = \int_0^{t_f} dt \tag{20}$$

$$subject\ \ to$$

$$\dot{\boldsymbol{r}}_I = \boldsymbol{v}_I \tag{21}$$

$$\dot{\boldsymbol{v}}_I = \frac{T}{m}\hat{\boldsymbol{u}} + \boldsymbol{g}(\boldsymbol{r}_I) \tag{22}$$

$$\dot{m} = -\frac{T}{g_0 I_{sp}} \tag{23}$$

$$\hat{\boldsymbol{u}}^T\hat{\boldsymbol{u}} = 1 \tag{24}$$

where $\boldsymbol{r}_I$, $\boldsymbol{v}_I$, and $\hat{\boldsymbol{u}}$ are the position, velocity, and thrust direction of the interceptor, respectively, $\boldsymbol{r}_I(0)$, $\boldsymbol{v}_I(0)$, and $m(0)$ are given, and $\boldsymbol{r}_I(t_f) = \boldsymbol{r}_d$ is final position. The final time, t_f, is not specified and the current time is set as zero.

Let us defined the Hamiltonian as

$$H = 1 + \boldsymbol{\lambda}_{\boldsymbol{r}}^T\boldsymbol{v}_I + \boldsymbol{\lambda}_{\boldsymbol{v}}^T(\frac{T}{m}\hat{\boldsymbol{u}} + \boldsymbol{g}(\boldsymbol{r}_I)) - \lambda_m\frac{T}{g_0 I_{sp}} + \mu_u(1 - \hat{\boldsymbol{u}}^T\hat{\boldsymbol{u}}) \tag{25}$$

Costate equations are represented as follows,

$$\frac{d\boldsymbol{\lambda}_{\boldsymbol{r}}}{dt} = -\left[\frac{\partial H}{\partial \boldsymbol{r}_I}\right]^T = -\left[\frac{\partial \boldsymbol{g}(\boldsymbol{r}_I)}{\partial \boldsymbol{r}_I}\right]^T \boldsymbol{\lambda}_{\boldsymbol{v}} \tag{26}$$

$$\frac{d\boldsymbol{\lambda}_{\boldsymbol{v}}}{dt} = -\left[\frac{\partial H}{\partial \boldsymbol{v}_I}\right]^T = -\boldsymbol{\lambda}_{\boldsymbol{r}} \tag{27}$$

$$\frac{d\lambda_m}{dt} = -\frac{\partial H}{\partial m} = \frac{T}{m^2}\boldsymbol{\lambda}_{\boldsymbol{v}}^T\hat{\boldsymbol{u}} \tag{28}$$

The optimality conditions are represented as

$$\left[\frac{\partial H}{\partial \hat{\boldsymbol{u}}}\right]^T = \frac{T}{m}\boldsymbol{\lambda}_{\boldsymbol{v}} - \mu_u\hat{\boldsymbol{u}} = 0 \tag{29}$$

DOI: 10.13009/EUCASS2023-357

$$\frac{\partial H}{\partial \mu} = 1 - \hat{\boldsymbol{u}}^T \hat{\boldsymbol{u}} = 0 \tag{30}$$

$$\frac{\partial^2 H}{\partial \hat{\boldsymbol{u}}^2} = -\mu_u I > 0 \tag{31}$$

From Eq. (29), the optimal control input can be obtained as

$$\hat{\boldsymbol{u}} = \frac{T}{m\mu_u}\boldsymbol{\lambda_v} \tag{32}$$

Note that the optimal control input $\hat{\boldsymbol{u}}$ is parallel to the costate vector $\boldsymbol{\lambda_v}$.

Assumption of the flat Earth yields the constant gravitational force, which implies that $\partial \boldsymbol{g}(\boldsymbol{r}_I)/\partial \boldsymbol{r}_I$ is zero. Therefore, $\boldsymbol{\lambda_r}$ becomes constant. Because there is only final position constraint, $\boldsymbol{\lambda_v}(t_f)$ becoms zero. As a result, $\boldsymbol{\lambda_v}$ can be written as

$$\boldsymbol{\lambda_v} = \boldsymbol{a}(t - t_f) \tag{33}$$

where $\boldsymbol{a}$ is a constant vector. Finally, the optimal control input can be obtained as a constant unit vector represented by

$$\hat{\boldsymbol{u}} = \frac{T}{m\mu_u}\boldsymbol{a}(t - t_f) = \hat{\boldsymbol{\lambda}} \tag{34}$$

The above optimal control problem is subject to two significant assumptions. Firstly, the assumption of the flat Earth is made. This assumption remains valid when changes in altitude are small relative to the radius of the Earth. Note that repeatedly employing a closed-form solution can yield reasonably accurate results.[12] Secondly, in Eq. (22), the influence of aerodynamic forces is neglected. As the proposed guidance law is applied to the middle stage of the multi-stage anti-ballistic missile, the interceptor using the proposed guidance law operates in both the endo-atmospheric and exo-atmospheric regions. Consequently, the presence of aerodynamic forces in the endo-atmospheric phase may produce some errors in time-to-go prediction. This issue will be addressed in the subsequent section.

3.2 Time-to-go Prediction

In this study, the interceptor consisting of three thrust phases, two coasting phases, and terminal phase is considered. Among the phases, the proposed guidance law is designed for the second thrust phase. Using the result that thrust guidance command is constant, the velocity of the interceptor can be predicted by integrating Eq. (22) as

$$\boldsymbol{v}_I(t) = \begin{cases} \boldsymbol{v}_I(0) + \int_0^t \frac{T}{m}\hat{\boldsymbol{u}}ds + \int_0^t \boldsymbol{g}(\boldsymbol{r}_I)ds, & 0 \le t < t_{b,1} \\ \boldsymbol{v}_I(0) + \int_0^{t_{b,1}} \frac{T}{m}\hat{\boldsymbol{u}}ds + \int_0^t \boldsymbol{g}(\boldsymbol{r}_I)ds, & t_{b,1} \le t < t_{b,1} + t_c \\ \boldsymbol{v}_I(0) + \int_0^{t_{b,1}} \frac{T}{m}\hat{\boldsymbol{u}}ds + \int_{t_{b,1}+t_c}^{t} \frac{T}{m}\hat{\boldsymbol{u}}ds + \int_0^t \boldsymbol{g}(\boldsymbol{r}_I)ds, & t_{b,1} + t_c \le t < t_{b,1} + t_c + t_{b,2} \\ \boldsymbol{v}_I(0) + \int_0^{t_{b,1}} \frac{T}{m}\hat{\boldsymbol{u}}ds + \int_{t_{b,1}+t_c}^{t_{b,1}+t_c+t_{b,2}} \frac{T}{m}\hat{\boldsymbol{u}}ds + \int_0^t \boldsymbol{g}(\boldsymbol{r}_I)ds, & t_{b,1} + t_c + t_{b,2} \le t \end{cases} \tag{35}$$

Based on the results, the position of the interceptor in the terminal phase can be predicted as follows,

$$\begin{aligned} \boldsymbol{r}_I(t) &= \boldsymbol{r}_I(0) + \int_0^t \boldsymbol{v}_I(0)ds + \int_0^t \int_0^s \boldsymbol{g}(\boldsymbol{r}_I)dlds + \int_0^{t_{b,1}} \int_0^s \frac{T}{m}\hat{\boldsymbol{u}}dlds + \int_{t_{b,1}}^{t_{b,1}+t_c} \int_0^{t_{b,1}} \frac{T}{m}\hat{\boldsymbol{u}}dlds \\ &\quad + \int_{t_{b,1}+t_c}^{t_{b,1}+t_c+t_{b,2}} \int_0^{t_{b,1}} \frac{T}{m}\hat{\boldsymbol{u}}dlds + \int_{t_{b,1}+t_c}^{t_{b,1}+t_c+t_{b,2}} \int_{t_{b,1}+t_c}^{s} \frac{T}{m}\hat{\boldsymbol{u}}dlds + \int_{t_{b,1}+t_c+t_{b,2}}^{t} \int_0^{t_{b,1}} \frac{T}{m}\hat{\boldsymbol{u}}dlds \\ &\quad + \int_{t_{b,1}+t_c+t_{b,2}}^{t} \int_{t_{b,1}+t_c}^{t_{b,1}+t_c+t_{b,2}} \frac{T}{m}\hat{\boldsymbol{u}}dlds \\ &= \boldsymbol{r}_I(0) + \boldsymbol{v}_I(0)t + \int_0^t \int_0^s \boldsymbol{g}(\boldsymbol{r}_I)dlds \\ &\quad + \left(S(t_{b,1}) + S(t_{b,2}) + L(t_{b,1})(t - t_{b,1}) + L(t_{b,2})(t - (t_{b,1} + t_c + t_{b,2}))\right)\hat{\boldsymbol{u}} \end{aligned} \tag{36}$$

where $t_{b,1}$ and $t_{b,2}$ are the remaining burn time of the solid propellant in the second and third stages, respectively, and t_c is the coasting phase between second and third stages. Note that current time is denoted as zero. The thrust integral parameters are obtained as follows,

$$L(t) = \int_0^t \frac{T}{m}dt = \int_0^t \frac{V_{ex}}{\tau - s}ds = V_{ex}\ln\frac{\tau}{\tau - t} \tag{37}$$

DOI: 10.13009/EUCASS2023-357

$$J(t) = \int_0^t \frac{T}{m} s ds = \int_0^t \frac{V_{ex} s}{\tau - s} ds = V_{ex} \left[\tau \ln \frac{\tau}{\tau - t} - t \right] \tag{38}$$

$$S(t) = \int_0^t \int_0^l \frac{T}{m} ds dl = \int_0^t \int_0^l \frac{V_{ex}}{\tau - s} ds dl = -V_{ex} \left[(\tau - t) \ln \frac{\tau}{\tau - t} - t \right] \tag{39}$$

$$Q(t) = \int_0^t \int_0^l \frac{T}{m} s ds dl = \int_0^t \int_0^l \frac{V_{ex} s}{\tau - s} ds dl = -V_{ex} \left[\frac{t^2}{2} + \tau \{ (\tau - t) \ln \frac{\tau}{\tau - t} - t \} \right] \tag{40}$$

where $\tau = -m(0)/\dot{m}$, and $V_{ex} = g_0 I_{sp} = -T/\dot{m}$.

To intercept the target by direct hit, the positions of the interceptor and the target after the time-to-go should be same, i.e.,

$$\boldsymbol{r}_I^{grav}(t_{go}) + (P t_{go} + Q)\hat{\boldsymbol{u}} = \boldsymbol{r}_T^{grav}(t_{go}) \tag{41}$$

where

$$\boldsymbol{r}^{grav}(t) = \boldsymbol{r}(0) + \boldsymbol{v}(0)t + \int_0^t \int_0^s \boldsymbol{g}(\boldsymbol{r}) dl ds \tag{42}$$

$$P = L(t_{b,1}) + L(t_{b,2}) \tag{43}$$

$$Q = S(t_{b,1}) + S(t_{b,2}) - L(t_{b,1}) t_{b,1} - L(t_{b,2})(t_{b,1} + t_c + t_{b,2}) \tag{44}$$

Because $\hat{\boldsymbol{u}}$ is a unit vector, following equation can be obtained from Eq. (41).

$$(P t_{go} + Q)^2 = \left(\boldsymbol{r}_T^{grav}(t_{go}) - \boldsymbol{r}_I^{grav}(t_{go}) \right)^T \left(\boldsymbol{r}_T^{grav}(t_{go}) - \boldsymbol{r}_I^{grav}(t_{go}) \right) \tag{45}$$

Assuming the flat Earth and using constant gravity obtained from the current position, Eq. (45) becomes a quartic equation for time-to-go as follows,

$$A_4 t_{go}^4 + A_3 t_{go}^3 + A_2 t_{go}^2 + A_1 t_{go} + A_0 = 0 \tag{46}$$

where

$$A_0 = \boldsymbol{r}_{TI}(0)^T \boldsymbol{r}_{TI}(0) - Q^2 \tag{47}$$

$$A_1 = 2\boldsymbol{v}_{TI}(0)^T \boldsymbol{r}_{TI}(0) - 2PQ \tag{48}$$

$$A_2 = \boldsymbol{g}_{TI}(0)^T \boldsymbol{r}_{TI}(0) + \boldsymbol{v}_{TI}(0)^T \boldsymbol{v}_{TI}(0) - P^2 \tag{49}$$

$$A_3 = \boldsymbol{g}_{TI}(0)^T \boldsymbol{v}_{TI}(0) \tag{50}$$

$$A_4 = \frac{1}{4} \boldsymbol{g}_{TI}(0)^T \boldsymbol{g}_{TI}(0) \tag{51}$$

with

$$\boldsymbol{r}_{TI}(t) = \boldsymbol{r}_T(t) - \boldsymbol{r}_I(t) \tag{52}$$

$$\boldsymbol{v}_{TI}(t) = \boldsymbol{v}_T(t) - \boldsymbol{v}_I(t) \tag{53}$$

$$\boldsymbol{g}_{TI}(t) = \boldsymbol{g}(\boldsymbol{r}_T(t)) - \boldsymbol{g}(\boldsymbol{r}_I(t)) \tag{54}$$

The time-to-go can be obtained by solving Eq. (46).

In the process of predicting the interceptor's position in the terminal phase, the influence of aerodynamic forces in the endo-atmosphere is neglected, and a constant thrust is used. Nevertheless, it is important to note that the feedback strategy implemented during the remaining engagement adequately compensates for the effects of aerodynamic forces and variations in thrust. This compensation is feasible because the interceptor, during the second stage, operates at high altitudes where the influence of aerodynamic forces is diminished. Furthermore, the assumption of the flat Earth does not significantly impact the computation of the guidance command, because it is performed using a feedback strategy.[12]

3.3 Guidance Command

Guidance command is obtained from Eq. (41) as follows,

$$\hat{\boldsymbol{u}} = \frac{\boldsymbol{r}_T^{grav}(t_{go}) - \boldsymbol{r}_I^{grav}(t_{go})}{\| \boldsymbol{r}_T^{grav}(t_{go}) - \boldsymbol{r}_I^{grav}(t_{go}) \|_2} \tag{55}$$

DOI: 10.13009/EUCASS2023-357

where

$$\boldsymbol{r}_T^{grav}(t_{go}) - \boldsymbol{r}_I^{grav}(t_{go}) = \boldsymbol{r}_{TI}(0) + \boldsymbol{v}_{TI}(0)t_{go} + \frac{1}{2}\boldsymbol{g}_{TI}(0)t_{go}^2 \tag{56}$$

The guidance command is aligned to the relative position of the target with respect to the interceptor after time-to-go where both the interceptor and target are assumed to be in free flight. Note that the positions of the interceptor and target are obtained using the constant gravitational acceleration and the current positions of the interceptor and target. As discussed in the previous sections, the error caused by the constant gravitational acceleration can be compensated by feedback strategy.

4. Numerical Simulation

4.1 Simulation Settings

The interceptor model used in the numerical simulation is adopted from ref. 1, which consists of three stages with solid propellant and an exo-atmospheric kill vehicle. The interceptor in the first stage and following coasting phase is operated in the endo-atmosphere. After that, the interceptor experiences both the endo-atmosphere and exo-atmosphere in the second stage, then it is operated in the exo-atmosphere during the rest of engagement. In this study, the numerical simulations are conducted from the second stage. The specifications of the interception are summarized in Table. 1.

Table 1: Specifications of the Interceptor.

Phase	m (kg)	T_{vac} (N)	I_{sp} (s)	A_e (m^2)	t_b (s)
Stage 2	5,815.1	157,854	291.8	0.5823	71.0
Stage 3	1,382.2	32,681	288.9	0.2171	66.8
Kill vehicle	64	-	-	-	-

4.2 Comparison of Guidance Law Performance

To evaluate the performance of the proposed guidance law, the performance of the proposed guidance law and that of the MZEM guidance law on the second stage are compared. Both methods use the MZEM guidance law for the third stage. To demonstrate the effectiveness of the proposed guidance law is, two different engagement geometries are considered. One is the head-on geometry where the target becomes closer to the launch point of the interceptor, and the other is the tail-chasing geometry where the target flies away from the launch point of the interceptor. The trajectories of each geometries are shown in Fig. 1. The dash line represents the trajectory from the beginning of the second stage to the beginning of the third stage.

In Fig. 1, it can be observed that the interception occurs earlier in the proposed guidance law than the MZEM guidance law, especially in tail-chasing geometry. Note that the MZEM guidance law assumes that both the interceptor and target are in free fall during the rest of the engagement. Therefore, the prediction errors of the time-to-go of the MZEM guidance law are larger than that of the proposed guidance law, as shown in Fig. 2. The appropriate prediction of time-to-go can put the interceptor at the appropriate position with adequate velocity at the start of third stage. If the midcourse guidance in the second stage is not properly performed, then the interceptor has to perform additional maneuver in the third stage, which may decrease the speed of the interceptor at the intercept and degrade the interception performance. Note that the larger speed at the intercept point, the higher the kill probability. The miss distances and the speeds of the interceptor at the intercept point are summarized in Table 2. For the proposed guidance law in the second stage, the miss distances are lower and the speed of the interceptor at the intercept point are higher than those of the MZEM guidance law for both the head-on and tail-chasing geometries.

Table 2: Miss distance and speed of the interceptor at the intercept point.

	Guidance law	Head-on	Tail-chasing
Miss distance (m)	MZEM	1.10	26.36
	Proposed	**0.14**	**3.33**
Speed of the interceptor at the intercept point (m/s)	MZEM	5,696.8	4,168.0
	Proposed	**6,294.4**	**5,405.7**

DOI: 10.13009/EUCASS2023-357

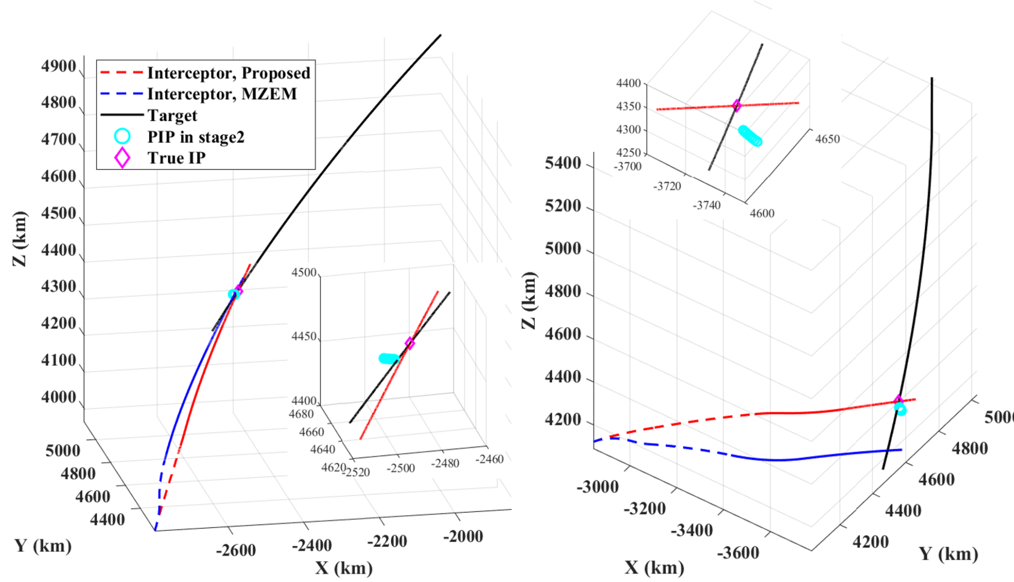

(a) Head on

(b) Tail chasing

Figure 1: Trajectories of the interceptor and target.

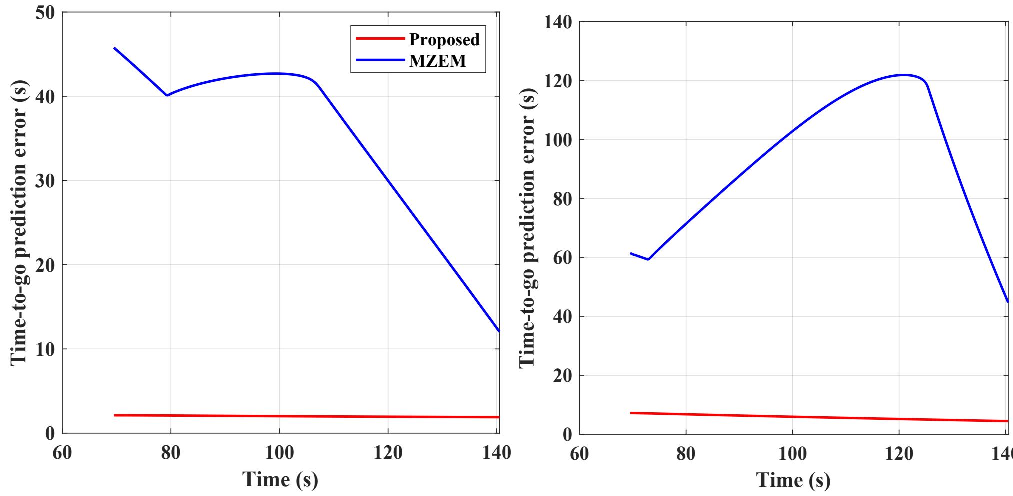

(a) Head on

(b) Tail chasing

Figure 2: Prediction error of time-to-go.

Figure 3 shows the response of the total angle of attack. The dash line represents the response from the beginning of the second stage to the beginning of the third stage. Non-response zone between the second and the third stage represents the coasting phase between the two stages. Because the MZEM guidance law computes the guidance command assuming no thrust in the rest of the engagement, total angle of attack at the beginning of the MZEM guidance law is large. Thus, using the proposed guidance law, the total angle of attack at the beginning of the third stage is large while the total angle of attack at the beginning of the second stage is large for the MZEM guidance law. In Fig. 3(a), the maximum total angles of attack for both guidance laws are similar, but for the MZEM guidance law, large total angle of attack is maintained for a little while, resulting in velocity loss. In Fig. 3(b), the total angle of attack for the MZEM guidance law is higher than that of the proposed guidance law not only in the second stage but also in the third stage. This is because in the tail-chasing geometry, the effect of the heading angle error at the beginning of the third stage is large. Thus, the proposed guidance law is more effective than the MZEM guidance law, especially when tail-chasing geometry.

DOI: 10.13009/EUCASS2023-357

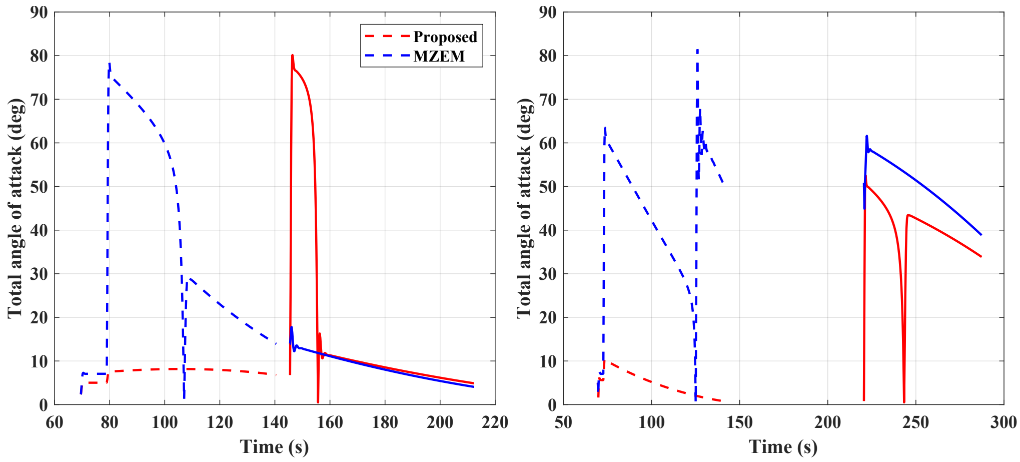

(a) Head on

(b) Tail chasing

Figure 3: Total angle of attack responses.

5. Conclusion

Midcourse guidance law for the second last stage was proposed. The proposed guidance law takes a feedback strategy without pre-computed data. Numerical simulations demonstrate that the intercept performance and the speed of the interceptor at the intercept point are improved for the proposed guidance law compared to modified zero-effort-miss guidance law. In this study, the interceptor consisting of three stages with solid propellant and an exo-atmospheric kill vehicle is considered. Modification of the guidance law for the interceptor with arbitrary configuration remains as future work.

6. Acknowledgments

This work was supported by Theater Defense Research Center funded by Defense Acquisition Program Administration under Grant UD200043CD

References

[1] Montero Yéboles, D., *Analysis and optimization of trajectories for ballistic missiles interception*, Ph. D. Dissertation, E.T.S.I. Aeronáuticos (UPM), Universidad Politécnica de Madrid, Madrid, Spain, Jan. 2016.

[2] Newman, B., "Strategic Intercept Midcourse Guidance Using Modified Zero Effort Miss Steering," *Journal of Guidance, Control, and Dynamics*, Vol. 19, No. 1, 1996, pp. 107–112.

[3] Zes, D., "Exo-atmospheric Intercept with J2 Correction," AIAA Guidance, Navigation, and Control Conference, Boston, MA, Aug. 1998.

[4] Ann, S., Lee, S., Kim, Y., and Ahn, J., "Midcourse Guidance for Exoatmospheric Interception Using Response Surface Based Trajectory Shaping," *IEEE Transactions on Aerospace and Electronic Systems*, Vol. 56, No. 5, 2020, pp. 3655–3673.

[5] Du, W., Chen, W., Yang, L., and Zhou, H., "Optimal Midcourse Guidance Algorithm for Exoatmospheric Interception Using Analytical Gradients," *International Journal of Aerospace Engineering*, Vol. 2019, Article ID 8502870, 9 2019.

[6] Zhao, S., Chen, W., Yang, L., and Wang, M., "Optimal Midcourse Guidance Law for the Exo-atmospheric Interceptor with Solid-propellant Booster," *Aerospace Science and Technology*, Vol. 127, Article ID 107670, 2022.

[7] Lee, J. Y., Jo, B. U., Moon, G. H., Tahk, M. J., and Ahn, J., "Intercept Point Prediction of Ballistic Missile Defense Using Neural Network Learning," *International Journal of Aeronautical and Space Sciences*, Vol. 21, No. 4, 2020, pp. 1092–1104.

DOI: 10.13009/EUCASS2023-357

[8] Song, E.-J. and Tahk, M.-J., “Real-time midcourse guidance with intercept point prediction,” *Control Engineering Practice*, Vol. 6, No. 8, 1998, pp. 957–967.

[9] Song, E.-J. and Tahk, M.-J., “Three-dimensional midcourse guidance using neural networks for interception of ballistic targets,” *IEEE Transactions on Aerospace and Electronic Systems*, Vol. 38, No. 2, 2002.

[10] Chen, Y.-W., “Dynamic interception point guidance algorithm based on particle swarm optimization,” *Measurement and Control*, Vol. 55, No. 9-10, 2022.

[11] Ann, S., Cho, N., Kim, Y., Shin, S., and Ahn, J., “Response Surface Modeling-based Analysis on Launch Vehicle Capability,” *Advances in Space Research*, Vol. 62, No. 12, 2018, pp. 3281–3297.

[12] Chandler, D. C. and Smith, I. E., “Development of the Iterative Guidance Mode with Its Application to Various Vehicles and Missions.” *Journal of Spacecraft and Rockets*, Vol. 4, No. 7, 1967, pp. 898–903.